FUNDAMENTALS OF AUTONOMOUS RELATIVE NAVIGATION AND ITS APPLICATION TO AERIAL REFUELING

Shahram Moafipoor*, Lydia Bock†, Jeffrey A. Fayman‡, David Honcik°

In this paper, we present the theoretical foundation and experimental results of a novel generic GPS/INS relative navigation system designed to support autonomous relative navigation of manned and unmanned UAVs in demanding applications such as aerial refueling, auto-landing, and formation operations. Although this paper presents a generic approach to relative navigation, emphasis is placed on the aerial refueling application. The objective is to provide relative position, velocity, and attitude between one or more refueling aircraft and the tanker. This information can be used by drogue control engineers to improve control law design.

The relative position, distance, azimuth and elevation of the line-of-sight vector from the refueling aircraft to the tanker are typically provided by vision or laser scanners. However, systems utilizing these sensors are complex and costly. We have developed a GPS-based system in which raw observations from the refueling aircraft are transmitted to the tanker through a data link. The tanker uses this data to determine its relative position to the refueling aircraft (or vise versa; depending on the control segment). The accuracy enhancement of the system is achieved by using the GPS carrier phase observable and fixing phase ambiguities. The line-of-sight relative position observation is used in a Relative Extended Kalman Filter, together with transmitted raw IMU data to provide relative navigation. We analyze the performance of the relative navigation system on real-world data. Two manned vehicles were equipped with independent GPS/IMU systems. A data link, operating in the 900 MHz. frequency band, was used to transfer the raw GPS and IMU data used in the Relative Extended Kalman Filter. To provide a "truth source" for evaluating the performance of the relative navigation solution, both autonomous GPS/IMU systems were fed data from an external reference receiver. The system provides up to 100 Hz. relative navigation data with an accuracy of 1.0 m position, 0.1 m/s velocity, and 0.5º attitude for all tests.

INTRODUCTION

Recent interest in manned and unmanned aerial vehicles (UAVs) has highlighted the importance of precise relative navigation information to the safe use of UAV's. Future military and civilian UAV applications will increasingly require capabilities such as sense and avoid, swarming, platooning, docking[1], autonomous landing[2], and autonomous aerial-refueling[3,4] all of which require access to accurate Relative Time Space Positioning Information (R-TSPI) between platforms. Traditionally, algorithms employing application specific approximations were developed to provide R-TSPI. For example, in aerial refueling it was assumed that the vehicles will be flying in close formation under similar dynamics[5].

* Navigation Scientist, PhD, Geodetics Inc, 2649 Ariane Dr, San Diego, CA, 92117, USA
† President and CEO, PhD, Geodetics Inc, 2649 Ariane Dr, San Diego, CA, 92117, USA
‡ VP Business and Product Development, PhD, Geodetics Inc, 2649 Ariane Dr, San Diego, CA, 92117, USA
° VP Software Development, Geodetics Inc, 2649 Aria ne Dr, San Diego, CA, 92117, USA

In this paper we present the theoretical foundation for a generic approach to relative navigation and the use of this technology for autonomous UAV aerial refueling. The approach is capable of meeting the full range of relative assisted manned and unmanned operations. We present a Relative Extended Kalman Filter (R-EKF) that integrates line-of-sight relative observations, including Global Positioning System (GPS)-based relative position and on-board sensors measuring relative bearing and/or relative distance. The system can provide up to 100 Hz R-TSPI with an accuracy of ±1.0 m position, ±0.1 m/s velocity, and ±0.5º attitude.

AERIAL REFUELING CHALLENGES

Automated Aerial refueling for UAV's is a challenging problem requiring accurate R-TSPI for safety of operation. Geodetics has developed the Geo-RelNAV® system, see Figure 1, to address this problem.

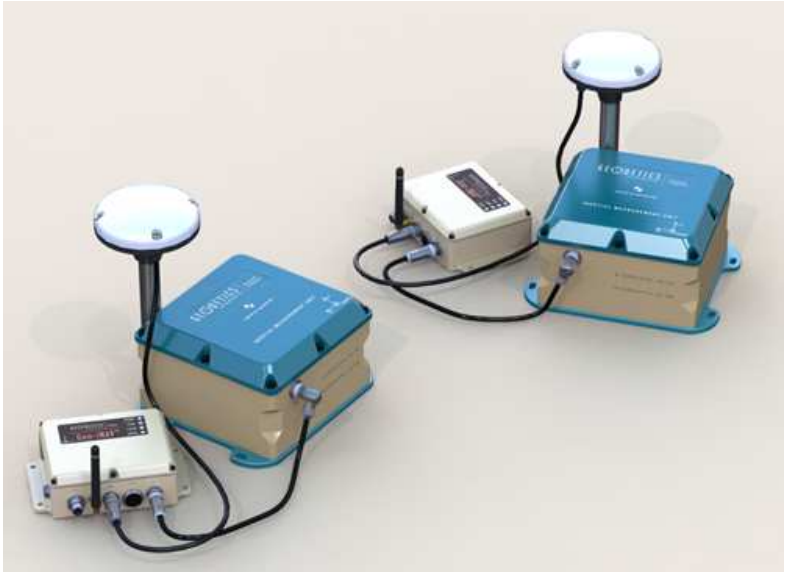

Figure 1: Geo-RelNAV

The navigation data provided by Geo-RelNAV can be critical for both safety and design improvements. An important measurement provided by Geo-RelNAV for the aerial refueling application is the vector closure rate, the differential velocity between the tanker and refueling aircraft. The closure rate is monitored in real time on-board the tanker. The measurement is used to: (1) maintain safety-of-flight by ensuring refueling airplanes do not exceed a certain speed, (2) determine whether or not a refueling airplane approached the tanker with sufficient speed, and (3) provide data to drogue control engineers to improve control law design.

Geo-RelNAV is configurable and natively provides solutions in the correct, non-inertial reference frame. It is a GPS/INS system, so an IMU can produce a navigation solution at a faster sample rate GPS alone. Solutions are available via UDP Ethernet providing a convenient way for analysis engineers to monitor the data in real-time using standard monitoring and recording tools. Geo-RelNAV can provide R-TSPI in different frames, including body-frame, local navigation frame (wander-azimuth) and earth-fixed frame, as well as transferring the solution to arbitrary points of interest on the aircraft such as the refueling aircraft's refueling probe.

RELATIVE INERTIAL NAVIGATION

In this paper, we use the terms Primary and Secondary to identify the platforms for which R-TSPI data is being generated. R-TSPI is always provided for the Primary with respect to the Secondary. Referring to Figure 2, the tanker is considered the Primary and the refueling aircraft, the Secondary (or vise versa; depending on the control segment). Data is always transmitted through the data link from the Secondary to the Primary. Figure 2 summarizes the geometric relations that will be used in the paper, where the Primary body frame is labeled *p-frame* and the Secondary body frame is labeled *s-frame*. The body frame fixed to the Primary (P) is shown by $\left(x_P^p, y_P^p, z_P^p\right)$, and body frame fixed to the Secondary (S) is shown by $\left(x_S^s, y_S^s, z_S^s\right)$.

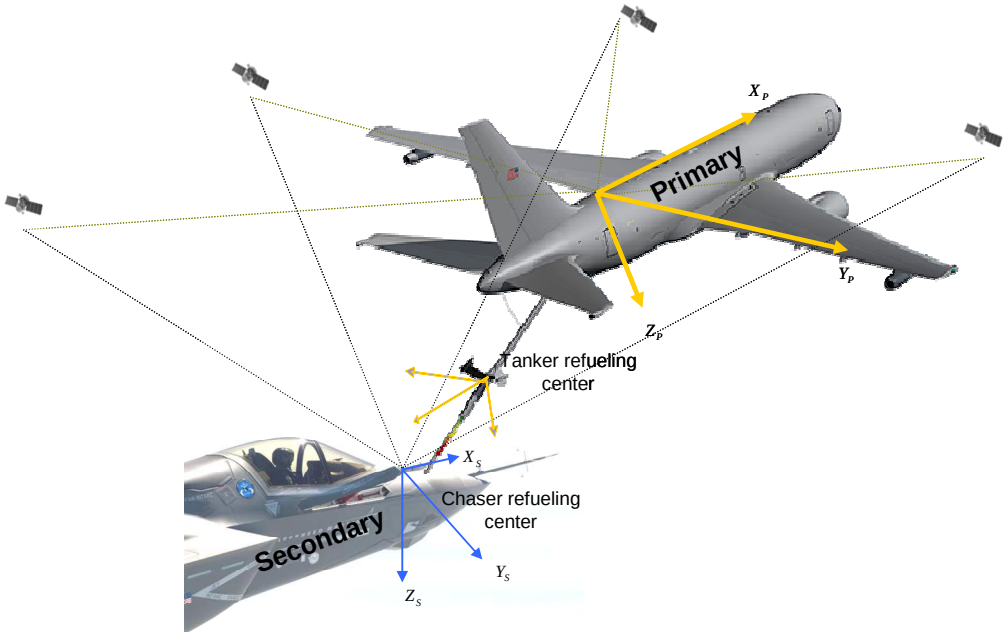

Figure 2: Primary/Secondary Geometry and Corresponding Body Frames Fixed to the Vehicle Body

The relative navigation equation is set up for the state of the Secondary with respect to the state of the Primary in the center of the body frame of the Primary, *p-frame*[6]:

$$\Delta\vec{X}_{PS}^{\,p} = \vec{X}_P^{\,p} - \vec{X}_S^{\,p} \tag{1}$$

where $\vec{x}_P^{\,p}$ is the Primary position vector established in the *p-frame*, and $\vec{x}_S^{\,p}$ is the Secondary position vector defined in the *p-frame*. Note that these vectors can also be obtained from the Primary/Secondary Strapdown inertial navigation solutions after transferring to the reference (eccentric) point. These vectors are transformed to the inertial frame, *i-frame*, using:

$$\Delta\vec{X}_{PS}^{\,p} = R_i^p\left(\vec{X}_P^{\,i} - \vec{X}_S^{\,i}\right) \tag{2}$$

where R_i^p is the Primary attitude matrix which transforms from the *i-frame* to the *p-frame*. Eq. (2) represents the fundamental equation, from which the relative navigation equations are derived.

This process is started by defining an interface frame, called *a-frame*, which is a completely arbitrary frame that rotates with respect to the *i-frame*[7]. Notice that in this application everything will be transformed to the body frame of the Primary, i.e., *a=p*. The relative position in the *a-frame* has coordinates in the *i-frame* given by:

$$\vec{X}^{i}_{P} - \vec{X}^{i}_{S} = R^{i}_{a}\left(\vec{X}^{a}_{P} - \vec{X}^{a}_{S}\right) = R^{i}_{a}\Delta\vec{X}^{a}_{PS} \tag{3}$$

Taking one time derivative of Eq. (3) yields the relative velocity dynamic model:

$$\Delta\dot{\vec{X}}^{i}_{PS} = \dot{R}^{i}_{a}\Delta\vec{X}^{a}_{PS} + R^{i}_{a}\Delta\dot{\vec{X}}^{a}_{PS} \tag{4}$$

In Eq. (4), the time derivative of the rotation matrix can be written as[7]:

$$\dot{R}^{i}_{a} = R^{i}_{a}\Omega^{a}_{ia} \tag{5}$$

where Ω^{a}_{ia} denotes a skew-symmetric matrix with elements from ω^{a}_{ia}, $\Omega^{i}_{ia} = [\omega^{a}_{ia}\times]$. Thus, Eq. (4) can be expressed as:

$$\Delta\dot{\vec{X}}^{i}_{PS} = R^{i}_{a}\Omega^{a}_{ia}\Delta\vec{X}^{a}_{PS} + R^{i}_{a}\Delta\dot{\vec{X}}^{a}_{PS} \tag{6}$$

Taking the second time derivative of Eq. (6) to obtain acceleration dynamic model, the relative acceleration equation in the *a-frame* is established as:

$$\Delta\ddot{\vec{X}}^{a}_{PS} = R^{a}_{i}\Delta\ddot{\vec{X}}^{i}_{PS} - 2\Omega^{a}_{ia}\Delta\dot{\vec{X}}^{a}_{PS} - \left(\dot{\Omega}^{a}_{ia} + \Omega^{a}_{ia}\Omega^{a}_{ia}\right)\Delta\vec{X}^{a}_{PS} \tag{7}$$

In Eq. (7), the forcing term, $\Delta\ddot{\vec{X}}^{a}_{PS}$, can be expressed by the Primary/Secondary accelerations sensed by their accelerometers, $\vec{a}^{p}_{P}, \vec{a}^{s}_{S}$, as:

$$\Delta\ddot{\vec{X}}^{i}_{PS} = \ddot{\vec{X}}^{i}_{P} - \ddot{\vec{X}}^{i}_{S} = \vec{a}^{i}_{S} + \vec{g}^{i}_{S} - (\vec{a}^{i}_{P} + \vec{g}^{i}_{P}) \tag{8}$$

where, $\vec{a}^{i}_{P}, \vec{a}^{i}_{S}$ are the specific forces, being also the quantity that is sensed by the Primary/Secondary accelerometers, respectively; and $\vec{g}^{i}_{P}(\vec{X}^{i}_{P}), \vec{g}^{i}_{S}(\vec{X}^{i}_{S})$ are the accelerations due to the gravitational fields in the *i-frame* and it is a function of the position vector for the Primary and Secondary, respectively. Using Eq. (8), Eq. (7) is given by:

$$\Delta\ddot{\vec{X}}^{a}_{PS} = R^{a}_{p}\vec{a}^{p}_{P} - R^{a}_{s}\vec{a}^{s}_{S} + R^{a}_{e}\left(\vec{g}^{e}_{P} - \vec{g}^{e}_{S}\right) - 2\Omega^{a}_{ia}\Delta\dot{\vec{X}}^{a}_{PS} - \left(\dot{\Omega}^{a}_{ia} + \Omega^{a}_{ia}\Omega^{a}_{ia}\right)\Delta\vec{X}^{a}_{PS} \tag{9}$$

To obtain the navigation equation in the *p-frame*, one might tempted simply to substitute '*a*' for '*p*' in Eq. (9)[8]. But, this would not provide the desired result, because the integration would

take place in a fixed frame[7]. The desire velocity vector is the *e-frame* velocity vector coordinatized in a frame parallel to the *p-frame*, which we denote as $\vec{V}_{PS}^{\,p}$, and it is given by:

$$\vec{V}_{PS}^{\,p} = R_e^p \Delta\dot{\vec{X}}_{PS}^{\,e} \tag{10}$$

The time-derivative of Eq. (10):

$$\frac{d}{dt}\vec{V}_{PS}^{\,p} = \dot{R}_e^p \Delta\dot{\vec{X}}_{PS}^{\,e} + R_e^p \Delta\ddot{\vec{X}}_{PS}^{\,e} \tag{11}$$

The $\Delta\ddot{\vec{X}}_{PS}^{\,e}$ can be obtained from Eq. (9) by specialized to *a*≡*e*:

$$\Delta\ddot{\vec{X}}_{PS}^{\,e} = R_p^e \vec{a}_P^{\,p} - R_s^e \vec{a}_S^{\,s} + \vec{g}_P^{\,e} - \vec{g}_S^{\,e} - 2\Omega_{ie}^e \Delta\dot{\vec{X}}_{PS}^{\,e} - \Omega_{ie}^e \Omega_{ie}^e \Delta\vec{X}_{PS}^{\,e} \tag{12}$$

Substitution Eq. (10) and Eq. (12) into Eq. (11) then yields the desire form of the relative navigation equation in the *p-frame* navigation equations.

Once the relative kinematic model of the position and velocity are established, the next step is to develop the relative attitude kinematic model[9]. The relative attitude, denoted by the quaternion q_s^p, is used to map vectors in the *s-frame* to vectors in the *p-frame*:

$$q_s^p = q_p^* \otimes q_s \tag{13}$$

where q_p and q_s are the quaternion attitudes of the Primary and Secondary with respect to the *i-frame*; q_p^* is the conjugate of q_p, and $\otimes$ is the quaternion multiplication operator. Following Eq. (13), the relative quaternion kinematic model can be summarized as:

$$\dot{q}_s^p(\xi) = \frac{1}{2} A\left(\omega_{ps}^s\right) q_s^p(\xi) \tag{14}$$

RELATIVE EXTENDED KALMAN FILTER

To establish the R-EKF, we need to derive the relative inertial error equations. The R-EKF has 21 basic states including 9 for relative position, $\delta\Delta\vec{x}_{PS}^{\,p}$, relative velocity, $\delta\vec{v}_{PS}^{\,p}$, and relative attitude, ψ_s^p, and 12 to model the Primary's gyro and accelerometer bias (non-constant) and non-linear scale factors. Since the relative distance between the Secondary and Primary is small compared to the radius of the Earth, the gravity terms, see Eq. (9), are negligible. Thus, in the linearized terms, the relative gravitational terms are ignored. It should be noted that the Secondary states are assumed to be known for retrieving the absolute Primary TSPI information. Since Equations (9), (11), and (14) can only provide the general dynamic model for a nonlinear state model, all these equations must be linearized using Taylor series about nominal values (neglecting the higher-order terms). After perturbation state equations are established, they should

be discretized from a continuous-time to a discrete-time sequence[6]. The final solution to the state equation can be expressed as:

$$\delta x^{p}_{PS}(t_k) = \Phi^{p}_{PS}(t_k, t_{k-1})\delta x^{p}_{PS}(t_{k-1}) + w(t_k) \tag{15}$$

with:

$$\Phi^{p}_{PS}(t_k, t_{k-1}) \cong I_{21\times 21} + F^{p}_{PS}.\Delta t$$

The perturbation elements are all related to the Primary:

$$\delta x^{p}_{PS} = \begin{bmatrix} \delta X^{p}_{PS}, & \delta v^{p}_{PS}, & \delta \Psi^{p}_{PS}, \\ \delta Accel^{p}_{Bias}, & \delta Accel^{p}_{Scale-Factor}, & \\ \delta Gyro^{p}_{Bias}, & \delta Gyro^{p}_{Scale-Factor} & \end{bmatrix} \tag{16}$$

The Jacobian F^{p}_{PS} matrix is established as:

$$F^{p}_{PS} = \begin{bmatrix} 0_{3\times3} & I_{3\times3} & 0_{3\times3} & 0_{3\times3} & 0_{3\times3} & 0_{3\times3} & 0_{3\times3} \\ F_{\Delta vp} & F_{\Delta vv} & F_{\Delta v\psi} & I_{3\times3} & F_{\Delta vA_{SF}} & F_{\Delta vG_B} & F_{\Delta vG_{SF}} \\ 0_{3\times3} & 0_{3\times3} & F_{\Delta\psi\psi} & 0_{3\times3} & 0_{3\times3} & I_{3\times3} & F_{\Delta\psi G_{SF}} \\ 0_{3\times3} & 0_{3\times3} & 0_{3\times3} & 0_{3\times3} & 0_{3\times3} & 0_{3\times3} & 0_{3\times3} \\ 0_{3\times3} & 0_{3\times3} & 0_{3\times3} & 0_{3\times3} & 0_{3\times3} & 0_{3\times3} & 0_{3\times3} \\ 0_{3\times3} & 0_{3\times3} & 0_{3\times3} & 0_{3\times3} & 0_{3\times3} & 0_{3\times3} & 0_{3\times3} \\ 0_{3\times3} & 0_{3\times3} & 0_{3\times3} & 0_{3\times3} & 0_{3\times3} & 0_{3\times3} & 0_{3\times3} \end{bmatrix} \tag{17}$$

RELATIVE GPS MEARSUREMENT MODEL

High-accuracy relative positions are derived from the use of carrier-phase differential GPS, a technique commonly used in static positioning applications such as surveying. However, unlike those applications, in this case the reference receiver is not stationary, it is located on a moving platform (Secondary). This is called the moving baseline problem. The relative GPS measurement in our system is provided by Geodetics' Epoch-by-Epoch® (EBE) differential carrier-phase processing[10], which measures accurate relative position between the Secondary and Primary systems. The EBE relative position has a typical accuracy better than 3 cm (1-sigma horizontal) and 6 cm (1-sigma vertical). To validate this, testing was conducted using two ground vehicles configured with 10 Hz. dual-frequency GPS sensors.

The real-time relative position solution was recorded onboard the Primary receiver (the Secondary vehicle was configured as the moving reference station). As a truth source for this test, we independently post-processed the data from the Secondary and the Primary GPS units and differenced the post-processed solutions. Figure 3 shows the solution and error plots of the two solution types North, East, and Up along with the statistical errors for each at the bottom of the plots. The outliers in the error plots correspond to points where the data link between the Primary and Secondary units was lost.

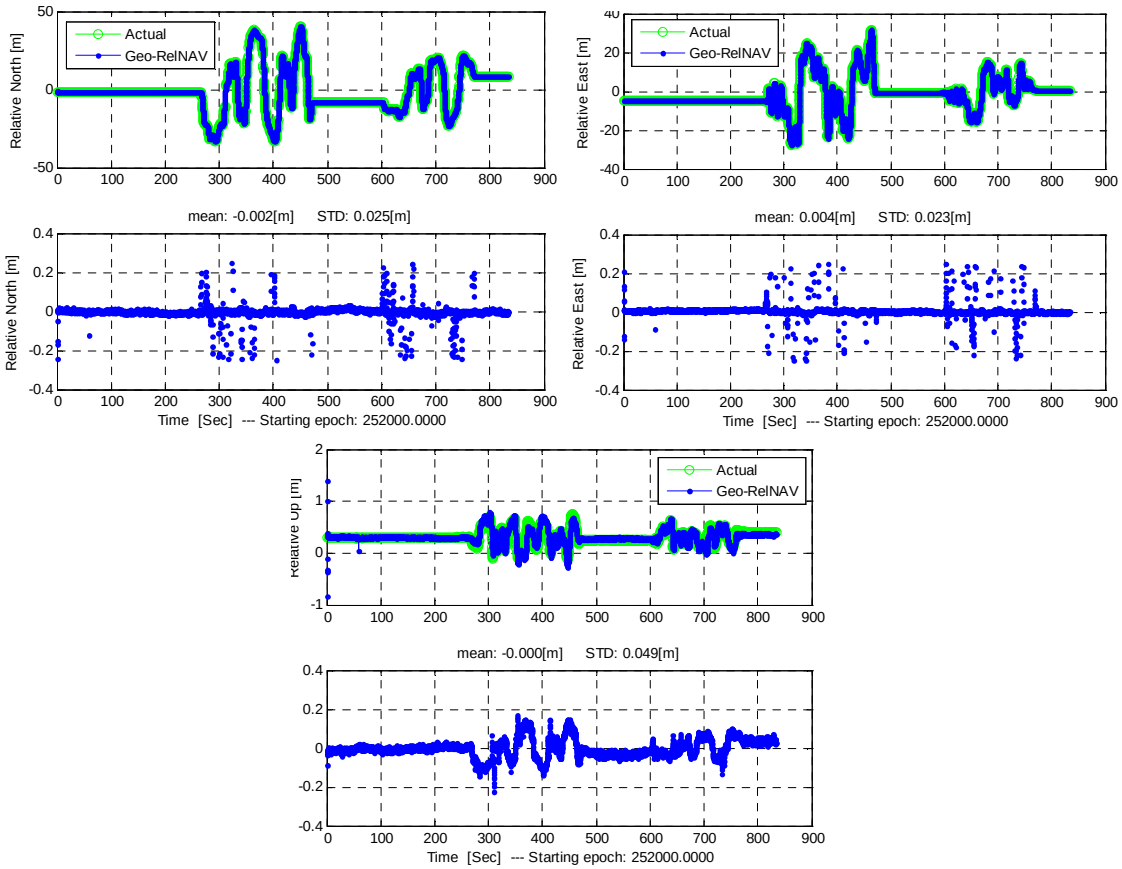

Figure 3: The Statistical Difference Between Real-Time Relative GPS Solution and Post-Processed Differential Relative GPS Solution

The mean difference is less than 5cm. Further investigation showed that a few large residuals were due to data link drop outs occurring at sharp turns. As a conclusion, the GPS relative mode was shown to provide accurate relative positions between the platforms.

Once the relative position is measured, the R-EKF observation model can be established as:

$$\vec{y}(t_k) = \left[\left(\Delta\vec{X}^{\,p}_{PS}\right)_{GPS} - \left(\Delta\vec{X}\right)_{INS}\right]_{(t_k)} \tag{17}$$

The $\left(\Delta\vec{X}^{\,p}_{PS}\right)_{GPS}$ is the relative position measured by using GPS data, and the $\left(\Delta\vec{X}^{\,p}_{PS}\right)_{INS}$ is the relative position, which is predicted by using the last updated inertial solutions, see Figure 4. Note that in order to use this relative observation, the lever-arm vector between the GPS and IMU of the both Primary and the Secondary must be accurately measured and applied. Here, the observation model is represented on the condition that the vector of observations, $\vec{y}(t_k)$, has yielded certain values based on an assumed linear relationship to $\Delta\delta X(t)$:

$$\vec{y}(t_k) = H\delta x^{p}_{PS}(t_k) + v(t_k) \tag{18}$$

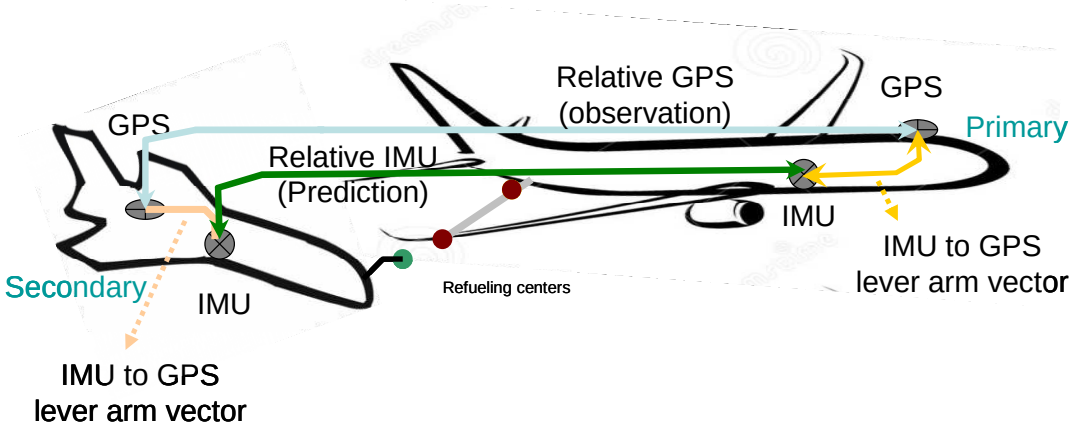

Figure 4: The Relative Observation Model

Eq. (15) and Eq. (18) are the fundamental equations of the R-EKF.

SYSTEM ARCHITECTURE

Relative navigation is computed and provided at one of the units, designated the Primary unit. This requires data from the Secondary unit to be transferred to the Primary unit over a data link. The Primary unit uses this transmitted data to calculate its position, velocity and attitude relative to the Secondary unit. Figure 5 summarizes the architecture and data-flow. Mathematically, the data from the Secondary unit used in the relative calculations are assumed to be errorless.

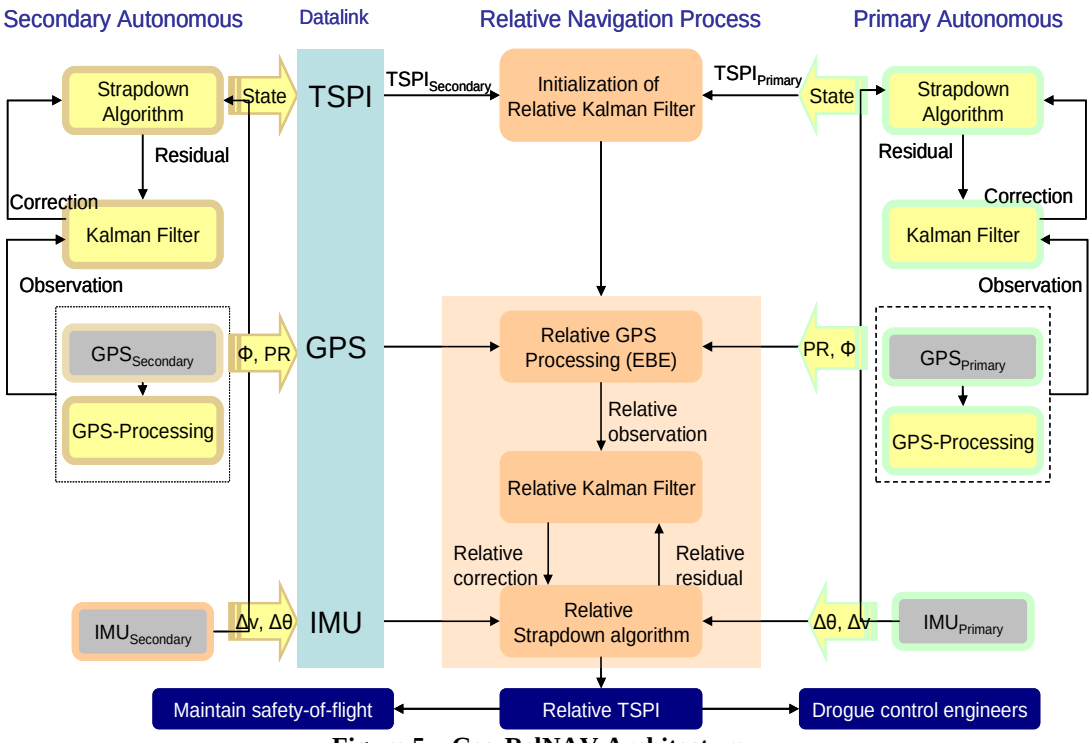

Figure 5 – Geo-RelNAV Architecture

OPERATIONAL ENVIRONMENT

We distinguish the following three relative navigation stages, illustrated in Figure 6, where each phase utilizes a unique processing mode.

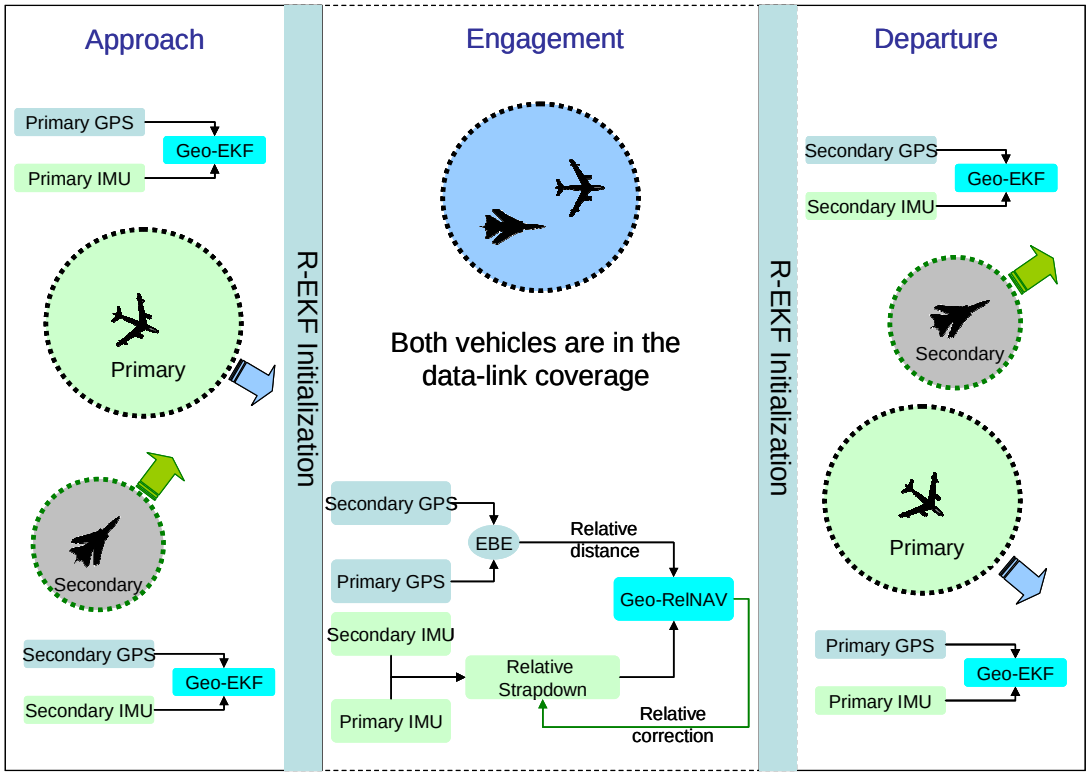

Figure 6 – Relative Navigation Phases

In the Approach phase, the data link between Primary and Secondary units is not closed. An autonomous navigation solution for both the Primary and Secondary units is computed on each platform independently. This information will be later used when the system transitions to the Engagement phase to initialize the R-EKF. In the Engagement phase, the data link between Primary and Secondary units is closed and the R-TSPI solution is computed between the platforms. Sensor observations are transmitted across the data link from the Secondary unit to the Primary unit. The Primary unit implements the R-EKF to produce the R-TSPI solution. In the Departure phase, the activity requiring R-TSPI is complete (i.e. refueling complete) and the Secondary platform pulls away from the Primary platform. In this phase, we transition from the R-EKF back to the autonomous independent navigation system.

The Approach phase is as important as the Engagement phase in attenuating the initialization error in terms of position, velocity, and attitude. To initialize the R-EKF, the autonomous TSPI solution from the Secondary unit is transferred to the Primary unit, where the initial relative position, velocity, and attitude are estimated. There are three conditions under which this initialization must occur: (1) upon transition from the Approach phase to the Engagement phase, (2) when in the Engagement phase and the system experiences a data link dropout, and (3) when there is a large latency in the data link. If the data link latency is too large, the data arriving at the Primary can no longer be used.

Data Link and Time Synchronization

Being an inertial navigation system, Geo-RelNAV relies on tight time synchronization of the IMU and GPS data in both Primary and Secondary units. Further, as a relative navigation system, data link latency must also be considered. The data link configuration for a specific radio will not be discussed here. However, the importance of data link bandwidth for the R-TSPI system cannot be over emphasized. Without data transmitted from the Secondary unit and received intact by the Primary unit, a R-TSPI solution can not be computed. Thus, the data link used should be carefully selected to provide sufficient bandwidth to support the desired update rate for the application.

There are three types of information transmitted from the Secondary unit: (1) raw GPS measurements, (2) raw IMU measurements, and (3) TSPI of the Secondary unit. The size of the GPS messages varies with the number of GPS satellites being tracked, a maximum of 600 bytes per message (dual-frequency observations) should be allocated. To help reduce the data link traffic, an algorithm was developed for down-sampling the IMU data from original rate (e.g., 100 Hz. for the Honeywell HG1700) to a lower rate for transmission (i.e., 20 Hz.). The size of the Secondary TSPI message is 102 bytes. As an example, the rates of 5 Hz. GPS and 20 Hz. IMU processing, requires a data link capable of transporting slightly over 5k Bps in one direction. If a higher throughput data link is in use, the change that would most improve system performance would be doubling the GPS sample rate to 10 Hz.

GEO-RELNAV VALIDATION TESTING

As part of the development process for Geo-RelNAV, several tests were conducted including static bench testing and dynamic ground vehicle testing. For static bench testing, Geo-RelNAV was setup on two points with a measured fixed displacement. The sensor configuration included dual-frequency GPS receivers, Honeywell HG1700 IMUs, and a data link operating in the 900 MHz. frequency band. Figure 7 (a-c) shows the R-TSPI solutions with statistical data analysis in the form of mean and standard deviation.

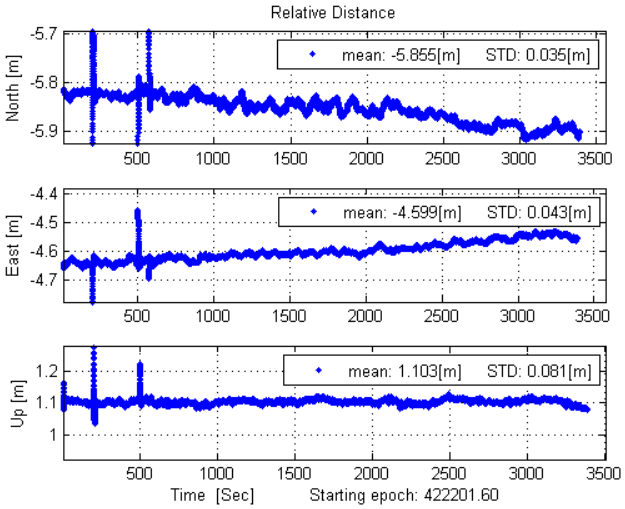

(a) Relative position

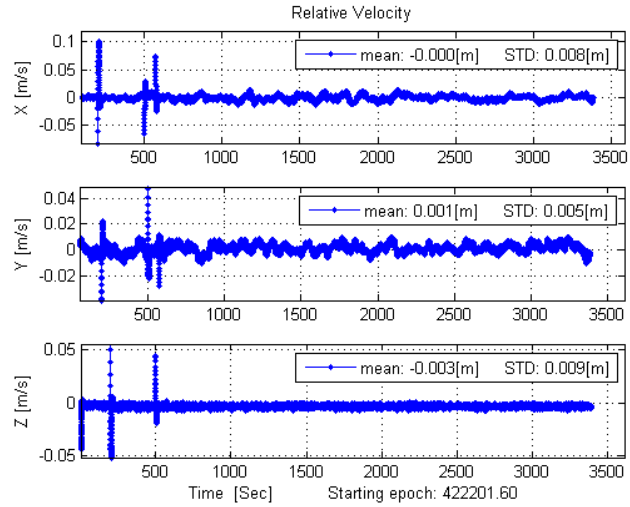

(b) Relative velocity

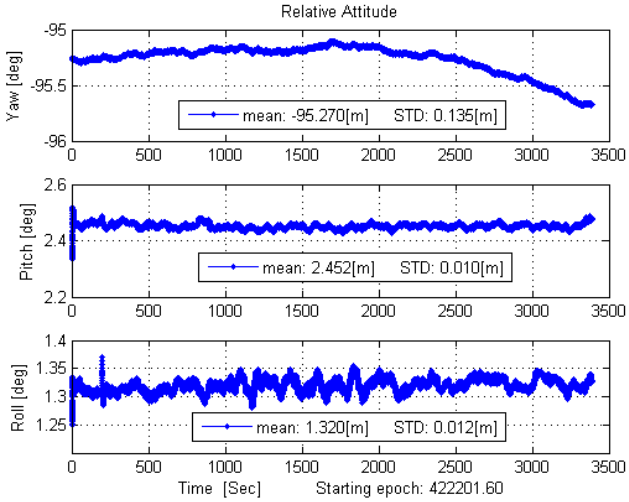

(c) Relative attitude

Figure 7: Relative Position, Velocity, and Attitude from Static Bench Test

The results of static bench testing illustrated in Figure 7 show that relative position held to the fixed offset with a standard deviation of less than 0.1 m in North, East and Up. Relative velocity held to zero with a standard deviation less than 0.01 m/s, and relative attitude was also maintained with the accuracy up to the gyro bias stability of HG1700 IMU (1°/Hr. for a stationary platform). The overall performance of the system in static bench test confirm the stability of the hardware and software of Geo-RelNAV, when the system is not exposed to any dynamics and the sensors are in close proximity (no data link latency or data dropouts).

Next, we moved to more realistic dynamic drive testing. To simulate the operational phases described in Figure 6, the drive test followed a scripted path. The two platforms left Geodetics' facility and drove separately (simulated Approach) until they met each other at the Fiesta Island test site (as shown in Figure 8), where the data link was closed for the Engagement phase. The Primary and Secondary navigation systems operated independently during the Approach phase.

Figure 8: Drive Test Ground Trajectory of the Primary (Blue) and Secondary (Red)

Once the data link was closed at the test site, the R-EKF engaged using initialization information transmitted from the Secondary to the Primary platform. To provide a "truth source" for evaluating the performance of the relative navigation solution, both autonomous GPS/IMU systems were fed data from an external reference receiver. Table 1 summarizes the statistic analysis of the R-TSPI solutions. Average RMS of fit in the relative position, velocity and attitude of approximately 1.0 m, 0.1 m/s and 0.3º, respectively, were computed for the entire relative navigation period. In this dynamic test, we encountered frequent data link dropouts, data link latency, as well as GPS outages, causing discontinuity in the R-EKF measurement updates until GPS was reacquired. During these periods, the R-EKF prediction model, updated with the last calibrated IMU data provided the R-TSPI. This test help confirm that the Geo-RelNAV performance is at the expected levels, even in the presence of real-world data link and GPS problems.

Table 1: Statistical Analysis of the R-TSPI Solution

R-TSPI Components		RMS Mean ± STD
Relative Position (m)	X_{PS}^{p}	0.1 ± 0.9
	Y_{PS}^{p}	0.1 ± 0.6
	Z_{PS}^{p}	0.2 ± 0.9
Relative Velocity (m/s)	ΔV_{x}^{p}	0.0 ± 0.1
	ΔV_{y}^{p}	0.0 ± 0.1
	ΔV_{z}^{p}	0.0 ± 0.1
Relative Attitude (degrees)	Yaw	0.0 ± 0.3
	Pitch	0.0 ± 0.1
	Roll	0.0 ± 0.1

CONCLUSION

We presented an autonomous relative navigation system and discussed its application for the aerial refueling problem. Considering the operational environment, special attention was placed on the system architecture so that the system can handle most possible real-world scenarios, including frequent data link dropouts, data link latency and GPS outages. The core of the system is a Relative Extended Kalman Filter, which uses GPS and IMU measurements of the Primary and Secondary platforms to estimate the relative inertial navigation states. The system is able to provide Relative TSPI at the IMU sample rate with an accuracy of ±1.0 m position, 0.1 m/s velocity, and ±0.5º attitude.

An added benefit of the system architecture is the ability to add observation models that do not rely on GPS. Thus, redundancy can be introduced using sensors such as vision systems. A generic format of relative observations, including relative range, bearing, and elevation is part of our future work.

REFERENCES

[1] B. Pervan, F., Chan, et al, "Performance Analysis of Carrier Phase DGPS Navigation for Shipboard Landing of Aircraft." Navigation. *Institute of Navigation.* Vol. 50, No. 3, 2003, pp.181-191.

[2] G. Xu, Y., Zhang, S., Ji, Y., Cheng, Y., Tian, "Research on Computer Vision-based for UAV Autonomous Landing on a Ship." *Pattern Recognition Letters.* Vol. 30, No.6, 2009, pp. 600-605.

[3] S. Khanafseh, S., B., Pervan, and G., Colby, "Carrier Phase DGPS for Autonomous Airborne Refueling." Proceedings of the ION NTM. San Diego, CA, 2005, pp. 489-499.

[4] W. Williamson, R., G. J., Glenn, V. T., Dang, et al., "Sensor Fusion Applied to Autonomous Aerial Refueling." *Guidance, Control, and Dynamics.* Vol. 32, No. 1, 2009, pp. 262-275.

[5] K., Liu et al, "Precision Relative Navigation Solution for Autonomous Operations in Close Proximity." IEEE/ION Plans, 2008, pp. 1246- 1251.

[6] S. Moafipoor, L. Bock and J.A. Fayman, "Manned and Unmanned Vehicle Relative Navigation System." Proceedings of ION GNSS. Nashville, TN, 2012, pp. 3512-3522.

[7] C. Jekeli, Inertial Navigation Systems with Geodetic Applications, Walter de Gruyter: Germany, 2001, pp: 124-140.

[8] A.M. Fosbury and J.L. Crassidis, "Kalman Filtering for Relative Inertial Navigation of Uninhabited Air Vehicles." AIAA Guidance, Navigation, and Control Conference and Exhibit, Keystone, Colorado, 2006, pp: 1-25.

[9] J.B. Kuipers, Quaternions and Rotation Sequences: A Primer with Applications to Orbits, Aerospace and Virtual Reality, Princeton University Press, 1999.

[10] P.J. de Jonge, Y. Bock, and M. Bevis, "Epoch-by-Epoch® Positioning and Navigation." Proceedings of ION GPS. Alexandria, VA, 200, pp: 337-342.